Preliminary Analysis of a Redundancy Resolution Method for Mobile Manipulators used in Physical Human Robot Interaction

Louis Fernandez, Marc G. Carmichael
University of Technology Sydney
louis.f.fernandez@student.uts.edu.au

Abstract

Adding mobility to a manipulator significantly increases its reachable workspace, allowing it to perform a wider variety of tasks. However, this advantage introduces the problem of expanding the system's solution space, resulting in an increase of different possible joint configurations for one specific end effector pose. Existing frameworks and algorithms have been developed that resolve this redundancy for a specific task. However, special care must be taken when mobile manipulators are used for Physical Human Robot Interaction (pHRI) applications. This paper proposes a basic framework utilising the Projected Gradient (PG) method that can be implemented on mobile manipulators used in pHRI. It illustrates how this redundancy resolution method has characteristics that makes it favourable for pHRI applications. The framework effectively makes use of the manipulator's high degree of precision when the task being executed is within its immediate workspace, while making use of the mobile platform's mobility when the task to be performed is outside of the manipulator's immediate workspace. This framework is validated firstly in simulation and then in a physical experiment. Both experiments successfully demonstrate the desired behaviour of a mobile manipulator system when used in the context of pHRI.

1 Introduction

For decades, industrial manipulators have been fenced away from their human counterparts to perform high volume and repetitive movements. However, due to several factors including technological advancement and the changing needs of industry, a new class of *collaborative* manipulator have emerged. Collaborative manipulators are able to be operated in shared spaces with humans, allowing the complementary strengths of both humans and robots to be combined to accomplish a common goal.

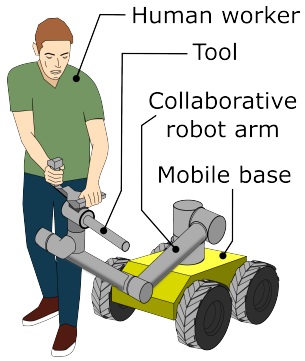

Figure 1: Example of mobile physical human-robot interaction

By mounting a collaborative manipulator on a mobile platform, a mobile collaborative manipulator like that depicted in Figure 1 can be formed. Mobile manipulators have great potential to be used in many areas due to the increase ability of the manipulator to reach a larger workspace. However, many factors must be taken into consideration to ensure that a suitable joint configuration is used for any given task. One such consideration is that the ability of the mobile platform to render accurate motions is often less than that of the manipulator due to hardware limitations, slipping of the wheels and errors in the mobile platform's kinematic model. Therefore, for tasks where the operator would like to execute trajectories solely within the manipulator's workspace, it is desirable to utilise only the joints of the manipulator. In contrast, when traversing between different tasks that is close to the limits or outside of the manipulator's workspace, it may be useful to utilise some or all of the mobile platform's degree of freedom so that manipulator singularities can be avoided and the task can be performed successfully. In this work we present a framework for redundancy resolution for mobile manipulators intended specifically for physical human robot interac-

tion (pHRI).

1.1 Related Literature

Redundancy resolution is the process of choosing a suitable solution within the many, potentially infinite, joint motions or configurations for a specific end effector task. Different redundancy resolution methods have existed since the late 1970s and have evolved over time to be used in specific applications. Examples include the use of Moore-Penrose Pseudoinverse (MPP), Extended Jacobian (EJ) [Nakamura, 1991], Projected Gradient (PG) [Liegeois, 1977], Reduced Gradient (RG) [De Luca and Oriolo, 1991] and Quadratic Programming (QP). All of which makes efficient and effective use of a system's redundancy for a given application. Throughout the decades, others have extended these methods for mobile manipulators with great success. [Seraji, 1998] demonstrated how adding the non-holonomic constraints and other user-defined kinematic constraints during task formulation allows for a more unified manner to control the motion of the mobile manipulator. [Haviland *et al.*, 2022] uses a holistic approach in modelling the mobile manipulator as well as QP to avoid the system's joint and velocity limits, and improve its manipulability throughout the desired trajectory. [De Luca *et al.*, 2006] presented an extension of the EJ, PG and RG methods on non-holonomic mobile manipulators and performed numerical studies to compare the performance of PG and RG methods. [Xing *et al.*, 2021a] used the PG method in a pHRI framework to provide assistance to the user by choosing an initial joint configuration that adds stiffness and compliance in the desired direction. [Xing *et al.*, 2021b] extends the work of [Flacco *et al.*, 2015] onto mobile manipulators. The paper used the concepts of saturation in the null space and stack of tasks to ensure that the joint configuration of the mobile manipulator is within the manipulator's joint, velocity and acceleration limits whilst simultaneously minimising the movement of the platform and maximising the manipulator's manipulability. In [Sorour *et al.*, 2019], a framework for controlling the motion of a mobile manipulator in a human shared environment was presented. In this work, a 'task sharing factor' was introduced which changes the weighting placed on the Jacobian depending on the task error. Therefore, the amount of contribution the mobile platform or manipulator has on the end effector motion can be controlled.

2 Problem Formulation

Existing redundancy resolution methods for mobile manipulators may often be unsuitable for pHRI applications. For instance, the use of MPP is undesirable as this solution minimises the velocity norm across all joints, resulting in substantial movement of the mobile platform when only motion of the manipulator is preferred. Unnecessary utilisation of the mobile platform may introduce kinematic inaccuracies in the system.

For conventional mobile manipulator applications that are not collaborative with humans, closed loop control using a sensor that estimates the end effector error is used to ensure the task is satisfied. Alternatively, in pHRI applications, the human operator becomes part of the closed loop control that ensures the task is executed successfully. In these cases, the movement of the mobile platform may be unnecessary, Moreover, it may even have a negative impact on the process as an unpredictable movement of the platform may cause a bizarre interaction between the human and the robot system. Additionally, unexpected motion of the platform or sudden switching between the manipulator and platform sub-systems may also reduce user confidence. As such, one of the challenges when using a mobile manipulator is the difficulty in controlling the level of involvement between the manipulator and mobile platform.

One solution to this problem is to use a weighted Jacobian where the weights are a function of the task error. If the task is beyond the workspace of the manipulator, the motion can be delegated to the mobile platform and the manipulator can perform a secondary task. [Sorour *et al.*, 2019] defined the secondary task to be a predetermined configuration that makes the manipulator take up less space and be more compact. [Xing *et al.*, 2021b] used the saturation in the nullspace method to choose between which subsystem is used to perform a given task. Both methods successfully chooses an optimal pose for their purpose that reduces the need for using the mobile platform. However, these methods may perform unsatisfactorily in a pHRI context. For instance, the knowledge of the desired task to be performed is often known only by the human operator and extracting this information is not straightforward.

This paper utilises the PG method to form a framework that has characteristics more suitable for pHRI applications. Compared to other methods, such as QP and RG, PG is a simple method which has the ability to demonstrate desirable characteristics that a redundancy resolution used in pHRI must have. Two different weighted Jacobian matrices are used as a way of choosing which subsystem is used to perform the desired motion. Similar to [Sorour *et al.*, 2019], the weightings of each Jacobian is a function of a metric related to the situation. In this paper, the metric is a function of manipulator manipulability rather than task error. The weighting function has the ability to smoothly transition the motion between the two subsystems to ensure comfortable interaction for the user. Furthermore, the weighting function, can be adjusted to potentially make better use of the mobile platform. For the rest of the paper, unless

specified otherwise, 'manipulability' refers to the manipulator manipulability rather than the manipulability of the whole system.

2.1 Kinematic Modelling and Motion Planning of a Mobile Manipulator

The simplest method for modelling a mobile manipulator is to augment the kinematic model of the mobile platform with the manipulators' kinematic model, often using DH parameters. In this paper, the kinematic model of the platform is modelled as a simple pair of prismatic joints along the x-y axes. An additional three revolute joint represent the manipulator mounted on the mobile platform.

The differential kinematics of the system is given by:

$$\dot{\boldsymbol{x}}(t) = \boldsymbol{J}(\boldsymbol{q})\dot{\boldsymbol{q}}(t), \tag{1}$$

where $\dot{\boldsymbol{x}}(t) \in \mathbb{R}^{n_t}$ is the motion of the end-effector which we refer to as the *task velocity*, $\dot{\boldsymbol{q}}(t) \in \mathbb{R}^{n_p+n_m}$ is the joint velocity vector, and $\boldsymbol{J}(\boldsymbol{q}) \in \mathbb{R}^{n_t \times (n_p+n_m)}$ is the Jacobian matrix. n_p and n_m denote the dimensions of the velocity vector of the mobile platform and manipulator, respectively, and n_t is the dimension of the task which often describes the end effector motion in Cartesian space.

2.2 Admittance Controller

An admittance controller is used to allow a human operator to directly control end effector movement through physical interaction. The virtual dynamics of the end effector motion with a mass-damper-spring model, is governed by the following general equation:

$$\boldsymbol{F}(t) = \boldsymbol{M}\ddot{\boldsymbol{x}} + \boldsymbol{C}\dot{\boldsymbol{x}} + \boldsymbol{K}\boldsymbol{x}, \tag{2}$$

where $\boldsymbol{M} \in \mathbb{R}^{n_t \times n_t}, \boldsymbol{C} \in \mathbb{R}^{n_t \times n_t}, \boldsymbol{K} \in \mathbb{R}^{n_t \times n_t}$ are positive definite matrices that represent task space inertia, damping and stiffness. It is noted that the spring stiffness is often set to zero, as is the case in this work.

The task velocity velocity $\dot{\boldsymbol{x}}$ is obtained by converting the force exerted on the manipulator's tool frame into a velocity command using the parameters of the admittance controller. The interaction forces can be measured by a force-torque sensor.

2.3 Redundancy Resolution

Given an end-effector velocity from the admittance controller, the redundancy resolution framework can be formulated through the following equations:

$$\dot{\boldsymbol{q}} = \boldsymbol{J}_w^+\dot{\boldsymbol{x}} + (\boldsymbol{I}_{n_p+n_m} - \boldsymbol{J}_{wm}^+\boldsymbol{J})\nabla\boldsymbol{q}_0, \tag{3}$$

$$\nabla\boldsymbol{q}_0 = \frac{\partial m}{\partial \boldsymbol{q}_k} = m \cdot trace(\frac{\partial \boldsymbol{J}}{\partial \boldsymbol{q}_k} \cdot \boldsymbol{J}^+) \tag{4}$$

$$\boldsymbol{J}_w^+ = \boldsymbol{W}^{-1/2}(\boldsymbol{J}\boldsymbol{W}^{-1/2})^+ \tag{5}$$

In this case, m is Yoshikawa's manipulability index [Yoshikawa, 1985], $\boldsymbol{J}^+$ is the traditional Moore-Penrose Pseudoinverse (MPP), $\boldsymbol{J}_w^+$ is a weighted pseudoinverse used to execute the primary task and $\boldsymbol{J}_{wm}^+$ is a different weighted pseudo-inverse for the secondary task. n_pandn_m represent the dimension of the mobile platform and manipulator, respectively.

The secondary task, $\nabla\boldsymbol{q}_0$, is defined to be manipulability maximisation. [Park *et al.*, 1999] describes a method that allows for the gradient of manipulability to be computed, which is described in Equation 4. The weighted pseudoinverse of the Jacobian matrices can be obtained from the relationship in Equation 5, introduced in [Chan and Dubey, 1995], where $\boldsymbol{W} \in \mathbb{R}^{(n_p+n_a)\times(n_p+n_a)}$ is a positive definite matrix. The given expression is able to find a solution even if the Jacobian is not full row rank, indicating the manipulator is close to or has reached a singularity.

As mentioned in the earlier sections, for mobile pHRI applications, it is often desirable to use the manipulator to execute the desired motion and only use the mobile platform when absolutely necessary. Manipulablity is a suitable metric for this application as the manipulability value is an indication of how well the manipulator is able to move in certain directions. High manipulability values suggest that the mobile platform does not need to be involved in the execution of the desired motion. In contrast, a lower manipulability suggests that the system is getting closer to a singularity and may require motion from the platform to successfully execute the desired motion. Furthermore, maximisation of manipulability was chosen to be the secondary task, with the aim of trying to maximise the motion of the manipulator only. In pHRI applications, low manipulability values can occur as the operator may not have knowledge of how driving the robot in certain configurations can result in a singular pose, for instance dragging the end effector close to the base of the manipulator. Therefore, trying to optimise the manipulability accounts for this and avoids having to use the mobile platform for the primary task.

Incorporating the manipulability in an exponential activation function helps determine the weighting matrix used for a given task and allow the mobile manipulator to transition smoothly between the manipulator and mobile platform. In general, the weighting matrix for the primary task can be defined as:

$$\boldsymbol{W} = \begin{bmatrix} (1-\gamma)\boldsymbol{I}_{n_p} & \boldsymbol{0}_{n_p \times n_m} \\ \boldsymbol{0}_{n_p \times n_m} & \gamma\boldsymbol{I}_{n_m} \end{bmatrix} \tag{6}$$

The top left matrix corresponds to the weighting values for the manipulator while the bottom right matrix

corresponds to the weighting values for the mobile platform. $\boldsymbol{I_d}$ is the identity matrix with dimension d. The exponential activation function, $\gamma \in [0, 1]$, is an exponential function that describes the weighting placed on the manipulator. It is given by the following equation:

$$\boldsymbol{\gamma} = \beta^{(m-m_a)/\tau} \tag{7}$$

where m is Yoshikawa's manipulability index, m_a is the minimum allowable manipulability and τ and β are parameters used for fine-tuning the function.

Analysing Equations 5, 6 and 7, it is evident that the weighting values for the two sub-systems have a inverse relationship and that a higher weighting value results in the corresponding joint being used less to execute the desired motion. As the manipulability of the manipulator approaches m_a, the closer the weighting value is to 1. Therefore, as the manipulability value worsens, the more that the manipulator motion is restricted and the mobile platform is used. Opting to use a weighted generalised matrix inverse over a conventional MPP allows for using the manipulator when the manipulability is high and using the mobile platform when manipulability is low. Similarly, using an oblique projector rather than the conventional orthogonal projectors, allows for using select joints to execute the secondary motion rather than minimising the norm across all the joints. This approach is akin to distributing the velocity of the primary and secondary motions to specific joints.

For the simplest case, the secondary weighting matrix $\boldsymbol{J}_{wm}^{+}$ can simply be a diagonal matrix consisting of 1s for elements corresponding to the mobile platform, and an arbitrary small number for elements corresponding to the manipulator. The reason for this is that the manipulator has a bigger impact on how the manipulability changes. Furthermore, the platform's motion when the manipulability is low will be unhindered and it can solely focus on the primary task. However, there is also the possibility of using a lower weight in the secondary Jacobian matrix corresponding to the the mobile platform. Since the secondary task is projected into the null space, any movement from the mobile platform will not impact the primary task and its lower kinematic accuracy will not affect the primary task. An alternative approach would then be to use an arbitrarily small value or γ for the mobile platform joints when the manipulability is high and increasing this value as the manipulability reduces. Furthermore, if the null space motion can continually maximise manipulability without interfering with the operator, then it avoids the need to use the mobile platform for executing the primary task.

3 Experimental Setup and Procedure

The efficacy of the proposed framework was evaluated firstly on simulation using Peter Corke's Robotic Toolbox on MATLAB [Corke, 2017]. Physical experiments were also performed using real mobile collaborative robot. The β and τ parameters for the experiments are illustrated in Table 1 and the joint activation parameter, γ, is plotted in Figure 2. Figure 2 illustrates how much the mobile platform is used as the manipulability of the manipulator changes. It can be observed that the simulation and physical experiment have vastly different joint activation functions. This is due to the fact that the manipulability of a 3 degree-of-freedom planar manipulator will largely differ to the manipulability of a 6 degree-of-freedom robot operating in 3D space. Therefore, the β and τ values must be adjusted accordingly. The joint activation functions used in the following experiments were chosen by examining the range of manipulability values of the robot systems being used. Once this range is known, different β and τ values were tested until a desired joint activation function was established for each case. For the simulation, the maximum manipulability value used was 2. For the physical experiment, the maximum manipulability value used was 1. In both cases, the minimum allowable manipulability was $10^{-}5$.

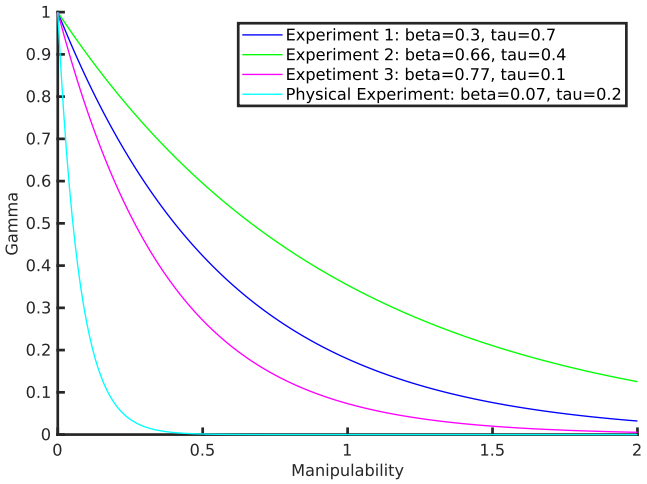

Figure 2: Plots of Different Joint Activation Functions

Table 1: Joint Activation Parameters

Experiments	$\boldsymbol{\beta}$	$\boldsymbol{\tau}$
Experiment 1 Value	0.3	0.7
Experiment 2 Value	0.66	0.4
Experiment 3 Value	0.77	0.1
Physical Experiment Value	0.07	0.2

3.1 Simulation

To evaluate the efficacy of the framework, a total of 5 simulations were performed. Experiments 1 and 2 each have one simulation each and were performed using the

Figure 3: Images during physical experiments with the mobile collaborative robot

proposed framework with different weights. A third simulation was performed using the MPP for comparison. Within all the simulations, a redundant 2D planar robot with 2 prismatic joints and 3 revolute joints was used. The prismatic joints represent a mobile platform, while the revolute joints represent the manipulator mounted on it. The task space has 3 dimensions corresponding to the x-y position and orientation of the end-effector, giving the system 2 degrees of freedom in the null space. The DH parameters are illustrated in Table 2. The planar robot and simulated environment can be seen in Figure 4

Table 2: DH Parameters

Joint	$\boldsymbol{\theta}$	**d**	**a**	$\boldsymbol{\alpha}$
Prismatic y	-pi/2	0	0	-pi/2
Prismatic x	-pi/2	0	0	-pi/2
Revolute 1	0	0	1	0
Revolute 2	0	0	1.3	0
Revolute 3	0	0	0.7	0

A predefined rectangular trajectory was used to examine how the mobile manipulator system would move when using the MPP and proposed framework. The trajectories were generated using 9 points and interpolated using a trapezoidal velocity profile. The x-y points, in order, are (1, 1.5), (-1, 1.5), (-1, 2.5), (1, 2.5), (1, 1.5), (-3.5, 3.5), (-3 3), (-1 3), (-1 2), (-3 2), (-3 3). When starting in the zero configuration, the initial rectangle, defined by the first four points, is well within the manipulator's reach. However, the second rectangle, defined by the last 4 points, include points which are well beyond the workspace of the manipulator. Therefore, the prismatic joints will need to be used to reach those points. Along with the traditional Moore-Penrose Pseudoinverse (MPP), the trajectory was executed using two sets of activation parameters, β and τ. This can be seen on Table 1 under Experiment 1 and Experiment 2.

Two more simulation, using the parameters in Experiment 3 under Table 1, were also performed using the same trajectory mentioned earlier. The aim of this analysis was to test the possibility of using lower weights for the secondary Jacobian to activate the mobile platform slightly more for improving manipulability. Therefore, one simulation was run using the simple method for choosing a weighting for the secondary Jacobian. For the final simulation, a more dynamic approach for the weights of the secondary Jacobian was used. The weights were γ for all joints while gamma is less than 0.4, approximately corresponding to values of manipulability greater than 0.4 as seen in Figure 2.

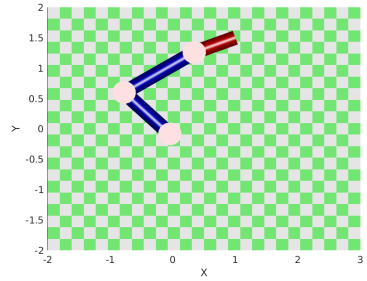

(a) Initial joint configuration when simulating with the MPP

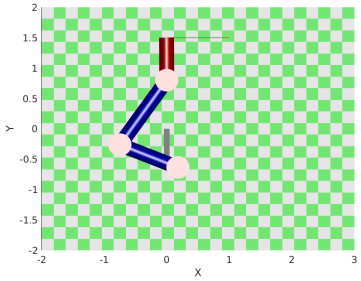

(b) Joint configuration at step 250 when simulating with the MPP

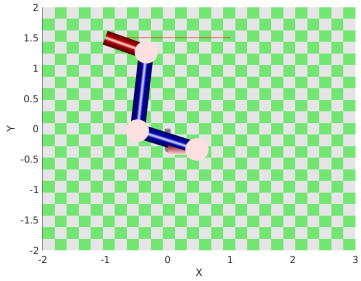

(c) Joint configuration at step 500 when simulating with the MPP

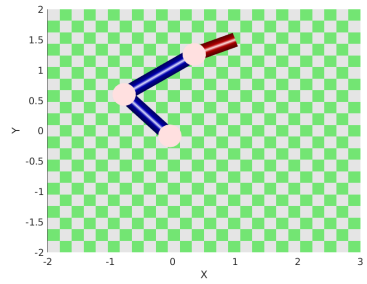

(d) Initial joint configuration for simulation 1

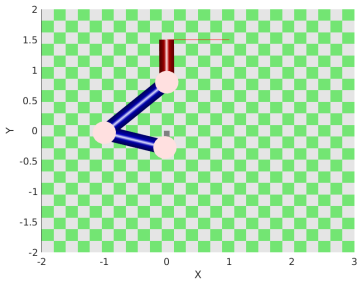

(e) Joint configuration at step 250 for simulation 1

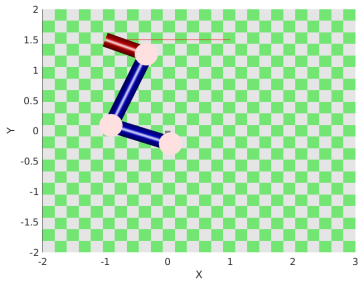

(f) Joint configuration at step 500 for simulation 1

Figure 4: Three joint configuration samples of the robot's motion for the first 500 steps. The blue segments represent the manipulator links and the red segment represents the manipulator's end effector. The red line is the trajectory that the end effector generated. Note that the manipulator's base is the white circle at the origin. Any segments that can be seen when the base moves away from the origin represents the prismatic x-y joints.

3.2 Physical experiment

The system used in the physical experiments was the RB-Vogui, a mobile platform with swerve steering consisting of independent drive and steer, with a UR10e 6-DoF lightweight collaborative robot mounted on top. The physical mobile manipulator system and screenshots of the physical experiment can be seen in Figure 3. To measure the interaction forces, the in-built force-torque sensor of the UR10e was used. A simple infinite impulse response filter was used to reduce any noise from the sensor.

The aim of this physical experiment is to validate the proposed framework on the real robot and demonstrate what a potential solution might look like for a redundancy resolution method used in pHRI. Therefore, the end effector of the UR10e was moved through arbitrary points in space using both the MPP and proposed framework. The admittance controller parameters used in this experiment are depicted in Table 3 and Table 1 depict the activation parameters used under Physical Experiment. For this experiment, the spring stiffness is set to zero.

Table 3: Admittance Controller Parameters

Parameters	**Linear**	**Rotational**
Mass Value	20 kg	1.176 $kg.m^2$
Damping Value	1/120 N/s	1/17 N.m/s

4 Results and Discussion

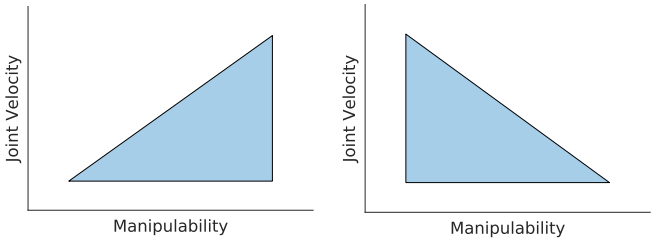

(a) Ideal 'Allowable' Joint Velocity for a Manipulator's Joint

(b) Ideal 'Allowable' Joint Velocity for a Mobile Platform's Joint

Figure 5: Ideal Joint Velocities

As mentioned in earlier sections, the aim of this framework is to only move the mobile platform unless absolutely necessary. More specifically, the mobile platform must not move unless the manipulator's joint(s) is ap-

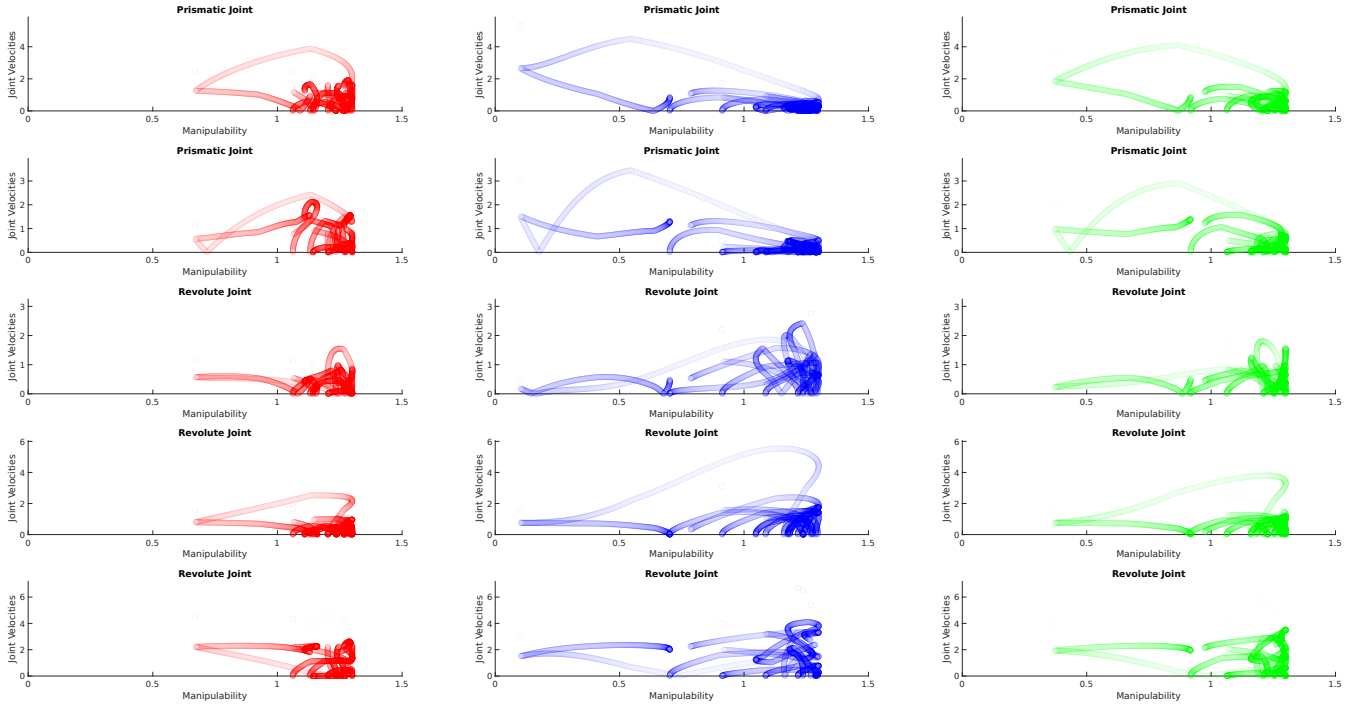

Figure 6: Velocity plots using MPP and the proposed framework using different weighting matrix. The column on the left (red) uses the conventional MPP solution while the blue plot (Experiment 1) and green plot (Experiment 2) uses the PG method

proaching a singularity in the direction that the end effector is moving towards. In the case where a manipulator's joint is moving towards a singularity, the proposed framework slowly 'activates' the mobile platform to move towards the desired Cartesian direction, whilst simultaneously reducing the contribution of the manipulator's joint which is approaching the singularity. For a more visual explanation, please refer to Figure 5a and Figure 5b. The area of the triangle represent the velocities that a specific joint should be able to execute at any point in time. Looking at Figure 5a, note how the manipulator joint is able to achieve higher velocities at higher manipulability values. However, as the manipulability decreases the velocities this joint can execute is generally reduced. However, the opposite is true for Figure 5b.

4.1 Simulation Results

The results of the first three simulations are illustrated in Figure 6, which plots *absolute joint velocity* against the manipulability of the manipulator. Absolute joint velocity is used since the direction that a joint is moving does not yield any useful information for the purpose of this experiment. Rather, the magnitude of the joint velocity gives insight as to how much a specific joint contributes to the system's motion. Note that the markers in the scatter plot have a certain level of transparency. This helps filter out any outliers or sudden changes in velocities indicated by a lone marker. It also assists in identifying areas of 'high density' since these areas will be darker as they have a larger number of markers. A high density area indicates that the mobile manipulator operated heavily in that region of manipulability. For instance, in Figure 6, there is a darker shade of blue at manipulability values around 1.2, indicating this is the manipulability region the system mostly operated in. Note also how the first two plots that corresponds to the prismatic joints have a flatter high density area, whereas the last three plots corresponding to the revolute joints have a taller high density area. This clearly demonstrates that the mobile platform's velocity is limited at higher manipulability values, allowing the manipulator's joints to contribute more to the execution of the task. However, the opposite is true as the manipulability drops. The manipulator's joint velocities quickly peak before the manipulability value reaches 1 and the mobile platform's velocity increases as the manipulability value decreases. This corresponds to the ideal joint velocity shapes in Figure 5.

The red scatter plots in Figure 6 represent the joint velocities executed when using the MPP. It is evident that the minimum norm property of this solution is undesirable as all the joints are set in motion despite the fact that the manipulator is capable of executing the given

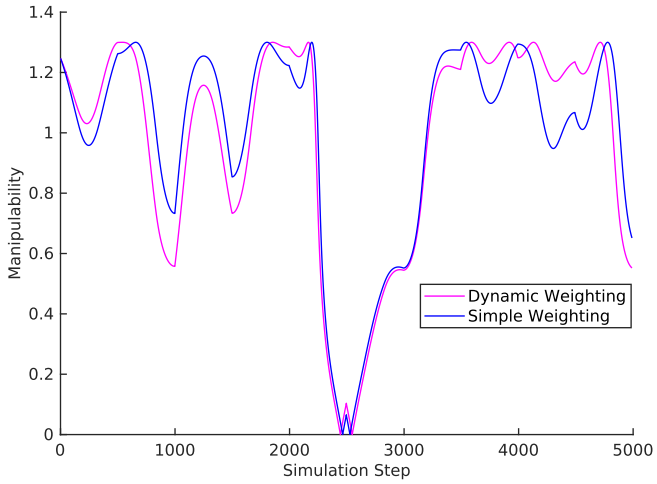

Figure 7: Manipulability Plots between the Simple and Dynamic Weights for the Secondary Jacobian

task, indicated by a high manipulability value. Based on the prismatic joints' taller high density region, it is clear that the mobile platform have a bigger contribution to the motion of the system when compared to the blue plots. It can also be seen from the plots that the ideal joint velocity shape is less evident as the manipulator joint velocities have a flatter high density area. Furthermore, this ideal shape is clearly contrdicted by the prismatic joint plots as the prismatic joint velocity peaks at such a high manipulability value.

Figure 4 contains images from the simulation which shows the configuration of the robot at three stages of the motion. Focusing on the two middle images. the vast difference between the proposed framework and MPP is clearly illustrated since the manipulator's base (indicated by the white circle which was initially at the origin), moves down the y-axis by about -0.5 in Figure 4b. In contrast to Figure 4e, the manipulator's base have minimal movement.

Looking at the green plots, which is somewhat similar to the MPP plots, it is clear that it uses the mobile platform even when the manipulability is relatively high. However, the activation of the mobile platform happens later compared to the MPP plots. For instance, the maximum absolute velocities for the prismatic joints are not achieved until after the manipulability drops to 1. Having this property, which allows the operator to tune when the platform is activated, is a desirable feature as it allows the user to change the behaviour of the system to suit their needs.

The results for the other simulations performed using the parameters in Experiment 3 is shown in Figure 7. It can be seen that the manipulability during the first half of the trajectory is slightly worse when using the dynamic weighting. However, there are points in the latter half where the manipulability for the dynamic weighting is greater than the simple weighting.

Similar results for the this experiment can also be obtained when the secondary velocity is scaled. Although, the manipulability dramatically drops at some points during the first half of the trajectory which cannot be justified with the improvement in the latter half. These results indicate that it may be possible to use the mobile platform for aiding the execution of the secondary task.

4.2 Physical Experiments Result

Videos for the proposed framework in action can be viewed at the following links:

- `https://youtu.be/4KxDJg1qzCg`
- `https://youtu.be/1MsIBVk4-bM`

A video of the MPP method being used can be viewed through this link:

- `https://youtu.be/u6SNxkaN0TE`

It should be noted that since the RB-vogui is a swerve robot, discrepancies exist between the software velocity output and the executed velocity of the RB-vogui. This discrepancy is due to the time it takes for the wheels to turn in the direction it is heading. In Figure 8, the software velocity output is plotted against the manipulability values. Similar to the earlier scatter plots, a certain level transparency is incorporated in the markers to show high density areas. The results in these scatter plots were obtained by dragging the UR10e's end effector towards the outer edges of its reachable workspace and then pushing the end effector back towards the UR10e's base. This way, the manipulator reaches an elbow singularity which forces the RB-vogui to execute the motion that the UR10e alone cannot execute. This is evident as the second prismatic joint's velocity (representing the RB-vogui's movement in the y-axis) increases as the manipulability value drops lower. Compared to joint 2 and joit 3 of the UR10e (representing the manipulator's elbow joints), their velocities decrease along with the manipulability value, with the joint velocity eventually reaching zero. Note how the joint velocities corresponding to the UR10e's shoulder and wrist joints, joint 1, 5 and 6, respectively, do not follow the ideal shape shown in Figure 5. This is because the singularity only affects the elbow joints and the UR10e is still able to move its end effector along the x-axis using the shoulder joint and change the end effector orientation using the wrist joints.

From the videos, it is clear that there is very little to no movement on the mobile platform while the UR10e is far from its singularities. However, once the UR10e reaches close to either an elbow or shoulder singularity, the mobile platform is activated. When the end effector is driven back towards a direction that contains higher

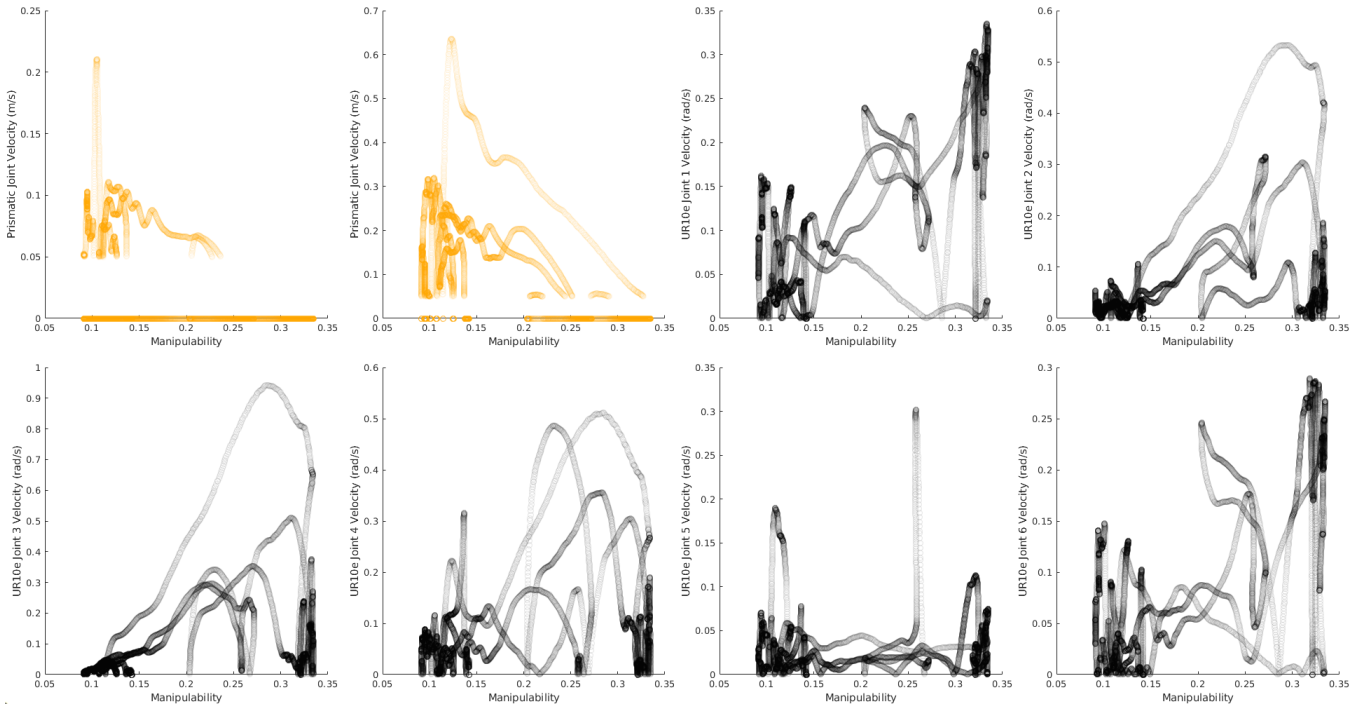

Figure 8: Manipulability and Joint Velocities Scatter Plots using the proposed method. The orange plots corresponds to the velocity for the RB-Vogui and the black plots corresponds to the velocities for the UR10e joints

manipulability values, the motion transitions smoothly between the manipulator and the mobile platform. In contrast, in the MPP solution, the RB-vogui is always involved in the execution of the desired motion regardless of the manipulator's configuration. Especially for such a large mobile platform that has such low stiffness in its mechanical design, it is undesirable to involve it in the motion as it results in continuous error during task execution. Furthermore, the forces produced by this low stiffness design is exacerbated the further the end-effector is from the UR10e's base. For this reason, it is essential that the manipulability of the system remains high to avoid the end-effector from reaching singularities, especially elbow singularities.

5 Conclusion and Future Works

In this paper, a redundancy resolution framework was introduced which clearly demonstrated the desired behaviour of a mobile manipulator system when used in the context of pHRI. To this end, two different weighted Jacobians were used to perform a primary and secondary task, which was projected into the null space of the system. The weighting of each Jacobian was defined in such a way that the mobile platform was not utilised unless absolutely necessary, defined by the manipulator's manipulability. The simulations verified that the framework was able to make use of the manipulator's high degree of precision when the task being executed is within the it's workspace whilst simultaneously avoiding singularities through the use of the prismatic joints, which represented a mobile platform. The physical experiments verified the efficacy of the framework when end-effector motion was controlled by a user. It also showed how the framework allows for smooth transition between the two subsystems.

Now that a conceptualised solution for a redundancy resolution method for pHRI applications have been developed, the reasoning behind the design choices used to create this framework can be used to guide more concrete solutions for such applications. Further work can also be done to improve the solution based on the challenges from this paper. For instance, note how the swerve model of the RB-vogui was not defined in the differential kinematic model, assuming wrongly that it is able to move in the desired heading instantaneously. Therefore, it will be helpful to define a more generalised model which incorporates the constraints on the mobile platform to create more fluid interaction between the user and the system. More importantly, note how the RB-vogui was not activated even in the slightest for improving manipulability. This is due to the lack of information that the model is receiving regarding the position of the user, which can cause motions that result in collision. To avoid this and improve the safety of the system, a collision avoidance scheme must be incorporated in the redundancy resolution method. Furthermore, to better

achieve the results in the second simulation, an alternative approach is to use a prioritised multi-task motion control where the robot can switch between the primary and secondary task. In combination with this, a RG approach rather than the PG approach can also be used to reduce the computational time of the framework. An alternative metric to replace the manipulability may also be helpful, especially for 6 degree-of-freedom manipulators. The manipulability is only a scalar value and lacks information regarding which joint and towards which direction the singularity occurs. Furthermore, the wrist singularities, which is incorporated in the manipulability value, is wasted information as the mobile platform cannot compensate for motions that change the orientation of the end effector. Therefore, a metric which consists of magnitude and directional information on the shoulder and elbow singularities may improve the efficiency of the proposed framework as no information is wasted.

References

[Chan and Dubey, 1995] Tan Fung Chan and R.V. Dubey. A weighted least-norm solution based scheme for avoiding joint limits for redundant joint manipulators. *IEEE Transactions on Robotics and Automation*, 11(2):286–292, 1995.

[Corke, 2017] Peter I. Corke. *Robotics, Vision & Control: Fundamental Algorithms in MATLAB*. Springer, second edition, 2017. ISBN 978-3-319-54413-7.

[De Luca and Oriolo, 1991] A. De Luca and G. Oriolo. The reduced gradient method for solving redundancy in robot arms. *Robotersysteme*, 7:117–122, 1991.

[De Luca *et al.*, 2006] A. De Luca, G. Oriolo, and P.R. Giordano. Kinematic modeling and redundancy resolution for nonholonomic mobile manipulators. In *Proceedings 2006 IEEE International Conference on Robotics and Automation, 2006. ICRA 2006.*, pages 1867–1873, 2006.

[Flacco *et al.*, 2015] Fabrizio Flacco, Alessandro De Luca, and Oussama Khatib. Control of redundant robots under hard joint constraints: Saturation in the null space. *IEEE Transactions on Robotics*, 31(3):637–654, 2015.

[Haviland *et al.*, 2022] Jesse Haviland, Niko Sünderhauf, and Peter Corke. A holistic approach to reactive mobile manipulation. *IEEE Robotics and Automation Letters*, 7(2):3122–3129, 2022.

[Liegeois, 1977] A. Liegeois. Automatic supervisory control of the configuration and behavior of multibody mechanisms. *IEEE Trans. Systems, Man, and Cybernetics*, 7(12):842–868, 1977.

[Nakamura, 1991] Yoshihiko Nakamura. *Advanced robotics - redundancy and optimization.* Addison-Wesley, 1991.

[Park *et al.*, 1999] Jong Hoon Park, Wan Kyun Chung, and Youngil Youm. Computation of gradient of manipulability for kinematically redundant manipulators including dual manipulators system. *Transaction on Control, Automation and Systems Engineering*, 1:8–15, 1999.

[Seraji, 1998] Homayoun Seraji. A unified approach to motion control of mobile manipulators. *Int. J. Robotics Res.*, 17(2):107–118, 1998.

[Sorour *et al.*, 2019] Mohamed Sorour, Andrea Cherubini, and Philippe Fraisse. Motion control for steerable wheeled mobile manipulation. In *2019 European Conference on Mobile Robots (ECMR)*, pages 1–7, 2019.

[Xing *et al.*, 2021a] Hongjun Xing, Ali Torabi, Liang Ding, Haibo Gao, Zongquan Deng, Vivian K. Mushahwar, and Mahdi Tavakoli. An admittance-controlled wheeled mobile manipulator for mobility assistance: Human–robot interaction estimation and redundancy resolution for enhanced force exertion ability. *Mechatronics*, 74:102497, 2021.

[Xing *et al.*, 2021b] Hongjun Xing, Ali Torabi, Haibo Gao, Weihua Li, and Mahdi Tavakoli. Enhancing kinematic accuracy of redundant wheeled mobile manipulators via adaptive motion planning. *Mechatronics*, 79:102639, 11 2021.

[Yoshikawa, 1985] Tsuneo Yoshikawa. Manipulability of robotic mechanisms. *The International Journal of Robotics Research*, 4(2):3–9, 1985.